Eur Radiol
DOI 10.1007/s00330-008-1251-z

ULTRASOUND

Guang-Jian Liu
Hui-Xiong Xu
Xiao-Yan Xie
Zuo-Feng Xu
Yan-Ling Zheng
Jin-Yu Liang
Ming-De Lu
Fuminori Moriyasu

Does the echogenicity of focal liver lesions on baseline gray-scale ultrasound interfere with the diagnostic performance of contrast-enhanced ultrasound?

Received: 4 September 2008
Accepted: 12 November 2008

G.-J. Liu · H.-X. Xu · X.-Y. Xie · Z.-F. Xu · Y.-L. Zheng · J.-Y. Liang
Department of Medical Ultrasound, Institute of Diagnostic and Interventional Ultrasound, The First Affiliated Hospital of Sun Yat-Sen University, Guangzhou, China

M.-D. Lu (✉)
Department of Hepatobiliary Surgery, Institute of Diagnostic and Interventional Ultrasound, The First Affiliated Hospital of Sun Yat-Sen University, 58 Zhongshan Road 2, Guangzhou, China 510080
e-mail: lumd@21cn.com
Tel.: +86-20-87765183
Fax: +86-20-87765183

F. Moriyasu
Department of Gastroenterology and Hepatology, Tokyo Medical University, 6-7-1 Nishi-Shinjuku, Shinjuku-ku, Tokyo 160-0023, Japan

Abstract The objective was to evaluate whether the echogenicity of focal liver lesions (FLLs) on baseline gray-scale ultrasound (US) interferes with the diagnostic performance of contrast-enhanced US (CEUS) for small FLLs. Three-hundred and eighty-eight patients were examined by real-time CEUS using a sulfur hexafluoride-filled microbubble contrast agent. The images of 114 hyperechoic lesions, 30 isoechoic lesions and 244 hypoechoic lesions were reviewed by two blinded independent readers. A five-point confidence level was used to discriminate malignant from benign lesions, and specific diagnoses were made. The diagnostic performances were evaluated by receiver-operating characteristic (ROC) analysis. The diagnostic performances of CEUS on hyperechoic lesions in terms of the areas (Az) under the ROC curve were 0.987 (reader 1) and 0.981 (reader 2), and were 0.987 (reader 1) and 0.984 (reader 2) for iso- and hypoechoic lesions, respectively. The sensitivity, specificity, positive predictive value, negative predictive value, and accuracy were 87.0–95.9%, 93.1–100%, 88.6–100%, 70.0–97.1% and 90.0–95.1%, respectively. The echogenicity of FLLs on baseline gray-scale US does not appear to interfere with the diagnostic ability of CEUS for small FLLs.

Keywords Echogenicity · Contrast agent · Focal liver lesion · Ultrasound

Introduction

The advent of low mechanical index (MI) contrast-enhanced ultrasound (CEUS) techniques and second-generation US contrast agents (UCA) provides us with a new noninvasive method of detecting and characterizing focal liver lesions (FLLs) in clinical practice. The enhancement patterns of different kinds of FLLs on CEUS have been well depicted, and the CEUS diagnostic performance on FLLs has been greatly improved compared with conventional gray-scale US, with 85–96% overall accuracy in differentiating malignant FLLs from benign ones and 81–88.5% overall accuracy in characterization of specific FLLs [1–6].

Contrast-specific US techniques are generally based on the cancellation and/or separation of linear US signals from tissue and utilization of the nonlinear response from UCA microbubbles. Most times, nonlinear harmonic US signals may still arise in tissues during sound wave propagation through the tissue, even though low MI real-time contrast-specific techniques may suppress tissue harmonic signals effectively [1, 7–9]. Therefore, insufficient suppression of tissue response by contrast-specific imaging, especially when the MI is relatively high in some circumstances, may degrade the imaging quality and cause erroneous interpretation of CEUS.

Recently, a paper reported that a kind of discordance between the enhancement pattern of FLLs on CEUS and

Published online: 10 January 2009

computed tomography (CT)/magnetic resonance imaging (MRI) is caused by fat in lesions, which shows hyperechogenicity on CEUS compared with its low attenuation on CT and low signal intensity on MRI [9]. It was presumed that the enhancement caused by the contrast agent is added to the baseline echogenicity of the FLLs containing fat and produced an erroneous interpretation of the degree of enhancement of the lesion.

This study aimed to assess whether the echogenicity of FLLs on baseline gray-scale US interferes with the diagnostic performance of real-time CEUS with a sulfur hexafluoride (SF6)-filled microbubble UCA.

Materials and methods

Patients

From March 2004 to Oct 2006, 388 patients with FLLs were retrospectively analyzed in this study. The inclusion criteria were as follows: (1) maximal lesion no larger than 3.0 cm in diameter; (2) lesion number less than 5; (3) no previously treated lesion; (4) no simple cystic lesion; (5) confirmed diagnosis by histopathology or clinical criteria. There were 272 men and 116 women with a mean age ± SD of 48.7±13.5 years (age range, 20–82 years). Among these 388 patients, 313 had a solitary lesion and 75 had multiple lesions. Only the most identifiable lesion on baseline gray-scale US was selected as the one to evaluate with CEUS when a patient had multiple lesions; thus, a total of 388 FLLs were evaluated in this study. The lesions were hyperechoic in 114, isoechoic in 30 and hypoechoic in 244 on baseline gray-scale US imaging. The maximal diameters of the lesions ranged from 0.9 to 3.0 cm (mean, 2.0± 0.6 cm). The final diagnoses of the lesions were 186 malignant and 202 benign FLLs, including 144 hepatocellular carcinomas (HCC), 37 metastatic liver cancers (MLC), 4 intrahepatic cholangiocarcinomas (ICC), 1 lymphoma, 77 hemangiomas, 28 focal nodular hyperplasias (FNH), 41 macro regenerative nodules (MRN), 6 focal fatty infiltrations, 35 focal fatty sparing, 3 dysplastic nodules, 6 inflammatory pseudotumors, 3 liver abscesses, 2 solid necrotic nodules, and 1 liver angioleiomyolipoma. Details of the echogenicities and final diagnosis of all the lesions were shown in Table 1.

The diagnoses of HCC were confirmed by histopathology in 83 lesions, with the specimens obtained by US-guided percutaneous biopsy (n=51) or surgery (n=32). The remaining 61 HCC lesions were confirmed by typical imaging findings on contrast-enhanced CT and/or MRI combined with positive laboratory data, such as hepatitis B or C and elevated serum α-fetoprotein level (over 400 ng/ml) [10]. Twenty-two MLC lesions were confirmed by histopathological examination, with the specimens obtained by percutaneous biopsy (n=14) or surgery (n=8), and the remaining 15 lesions were confirmed by clinical data such as history of the primary malignancy, newly detected and continuously enlarged FLLs, and typical imaging findings on contrast-enhanced CT/MRI [2, 3, 5]. The metastases were secondary to colorectal carcinoma (n=27), pancreatic carcinoma (n=4), breast carcinoma (n=1), gastric carcinoma (n=1), gastric leiomyosarcoma (n=1), duodenal papilla carcinoma (n=1), renal carcinoma (n=1), and unknown primary cancer (n=1). The ICC lesions were confirmed histopathologically with the specimens obtained by US-guided percutaneous biopsy (n=2) or surgery (n=2). All the hemangiomas were proved by characteristic findings on contrast-enhanced CT/MRI and lack of change in lesion size for at least 6 months on imaging follow-up [2, 5]. All the lesions of FNH, MRN, dysplastic nodule, focal fatty infiltration or sparing, inflammatory pseudotumor, liver abscess, solid necrotic nodule, liver angioleiomyolipoma and hepatic lymphoma were confirmed by US-guided percutaneous biopsy and imaging follow-up for at least 6 months. Informed consents for the entire procedures were obtained from all the patients.

Table 1 Echogenicity of focal liver lesions on baseline gray-scale US

Entity	Hyperechoic	Isoechoic	Hypoechoic	Total
HCC	30	20	94	144
MLC	11	2	24	37
ICC	1	1	2	4
Lymphoma	–	–	1	1
Hemangiomas	45	3	29	77
FNH	1	2	25	28
MRN	18	2	21	41
Focal fatty infiltration/sparing	6	–	35	41
Dysplastic nodule	–	–	3	3
Abscess	–	–	3	3
Inflammatory pseudotumor	1	–	5	6
Solid necrotic nodule	–	–	2	2
Angiomyolipoma	1	–	–	1
Total	114	30	244	388

Contrast-enhanced sonography

The US machines and contrast-specific software used in this study were an Acuson Sequoia 512 machine with contrast-pulse sequencing (CPS) software (Siemens Medical Solutions, Mountain View, Calif.) and an Aplio XV scanner with contrast harmonic imaging (CHI) software (Toshiba Medical Systems, Tokyo, Japan). Detail parameters were shown in Table 2. Seventeen patients were performed with CHI techniques and 371 patients with CPS techniques in the present study. The contrast agent used in

Table 2 Settings of the US equipment

Parameter	Specification/setting	
Machine type	Acuson Sequoia 512	Toshiba Aplio XV
Transducer	4 V1 vector transducer,1–4 MHz	375 BT convex transducer, 3.5 MHz
Imaging mode	Contrast pulse sequencing	Contrast harmonic imaging
MI	0.1–0.19 (as read on screen)	0.06–0.10 (as read on screen)
Frequency (MHz)	1.5, 2.0	2.5, 3.5
Frame rate (Hz)	8	10, 17
Gain	Auto adjust	Auto adjust
TGC curve	Positioned at center	Positioned at center
Depth (cm)	5–16	8–15
Focus position	Bottom of the lesion	Bottom of the lesion
Focus number	2	1

the present study was an SF6-filled microbubble contrast agent (SonoVue, Bracco, Milan, Italy).

In the CPS technique, a series of three pulses that differ in amplitude and phase is sent along each line, and through an acceptable combination of these pulses, microbubble-specific nonlinear fundamental and harmonic US frequencies are imaged. While CHI technique relies on transmitting a pair of acoustic pulses of opposite phase at low acoustic pressures and then summing the received signal. The linear echoes from tissue are cancelled during summation, whereas nonlinear echoes from microbubbles are summed coherently. Both of these techniques allow continuous low MI imaging with a high microbubble-tissue ratio and spatial resolution [2, 7–9].

Before administration of the UCA, baseline gray-scale US was performed to scan the liver thoroughly. The imaging settings of the US scanners were optimized to get the best depiction of the target lesion. The diagnostic information, including the diameter, echogenicity, shape and margin of each lesion, was recorded. After initiation of contrast-specific imaging mode, the imaging settings including the gain, depth, and focus, were readjusted to best visualize the target lesion and surrounding liver parenchyma. A volume of 2.4 ml of contrast agent was injected into the antecubital vein in a bolus fashion through a 20-gauge intravenous cannula, followed by a flush of 5 ml of 0.9% normal saline solution. The timer was activated simultaneously at the beginning of UCA administration. The lesion was observed continuously for 6 min under contrast-specific imaging. According to previous reports, the arterial phase was defined as 8–30 s after contrast-agent injection, the portal phase as 31–120 s, and the late phase as 121–360 s [1–5]. Both the digital cine clips of baseline gray-scale US and the whole process of CEUS images were stored in the hard disk incorporated in the scanner and were converted from DICOM files into low compressed AVI files for subsequent analysis on a personal computer. No patient received an additional administration of the contrast agent in this study. All baseline gray-scale US and CEUS were performed by one of two skilled investigators with at least 3 years' experiences of CEUS.

Image analysis

Digital cine clips of baseline and CEUS image were retrospectively analyzed in a randomized order by two independent readers who had at least 5 years' experience in CEUS of the liver, were not involved in the scanning, and were blind to clinical, histopathological and other imaging results. After reviewing the images, the readers were asked to make a diagnosis of benignity or malignance for each lesion. The grade of enhancement on CEUS was divided into hypoenhancement, isoenhancement and hyperenhancement compared with the surrounding liver parenchyma. Hyperenhancement in the arterial phase with complete washout in portal and late phase was diagnostic criteria for malignant lesion; hyper- or isoenhancement in arterial phase without washout in portal and late phase was diagnostic criteria for benign lesion. The diagnostic confidence was graded by a five-point scale: 1, definitely benign; 2, probably benign; 3, indeterminate; 4, probably malignant; 5, definitely malignant [2, 3, 5]. Then the readers were asked to make a specific diagnosis according to the well-established diagnostic criteria described in previous reports [1–5].

Statistical analysis

All the FLLs were divided into two groups according to their echogenicities on baseline gray-scale US as hyperechoic group and iso-/hypoechoic group. The grade of

Table 3 Enhancement level of benign focal liver lesions on different vascular phases

Baseline US	Reader	Arterial phase			Portal phase			Late phase		
		Hyper	Iso	Hypo	Hyper	Iso	Hypo	Hyper	Iso	Hypo
Hyperechoic	1	48	23	1	37	33	2	34	33	5
	2	50	21	1	36	34	2	35	33	4
Isoechoic	1	5	2	0	5	2	0	5	2	0
	2	5	2	0	5	2	0	5	2	0
Hypoechoic	1	66	53	2	35	76	10	34	77	10
	2	68	51	2	36	75	10	34	76	11
P	1	0.517			0.007[a]			0.025[a]		
	2	0.444			0.015[a]			0.017[a]		

[a]Statistically significant difference

enhancement of FLLs with different echogenicity on baseline gray-scale US was compared by the χ^2 test. The diagnostic confidence in differentiating benign FLLs from malignant FLLs with different echogenicity on baseline gray-scale US was assessed by a receiver-operating characteristic (ROC) curve, and the diagnostic performance was expressed as area under the ROC curve (Az). Interobserver agreement in diagnostic performance was evaluated by weighted κ statistics. Agreement was graded as poor (κ<0.20), moderate (κ=0.20 to <0.40), fair (κ= 0.40 to <0.60), good (κ=0.60 to <0.80), or very good (κ= 0.80–1.00). According to the rule that lesions assigned a confidence grade of 4 or 5 were defined as positive results, and those assigned a confidence grade of 3 or less were defined as negative results, the sensitivity, specificity, positive predictive value (PPV), negative predictive value (NPV) and accuracy were calculated with respect to echogenicity of FLLs on baseline gray-scale US. The relationship between correctly characterized FLLs with different echogenicity on baseline gray-scale US was assessed by the χ^2 test. A *P* value less than 0.05 was considered a statistically significant difference. The statistical analyses were performed using the SPSS 11.0 software package (SPSS, Chicago, Ill.).

Results

Enhancement of the FLL and surrounding liver parenchyma in every patient of the present study was depicted well by CEUS imaging. As to the grade of enhancement of benign FLLs, there was no significant difference between the hyperechoic group and iso-/hypoechoic group on the arterial phase ($P>0.05$ for both readers, χ^2 test); while significant differences were shown between the two groups in case of the grade of enhancement on the portal and late phases ($P<0.05$ for both readers, χ^2 test). With regard to the malignant FLLs, the grade of enhancement during all the vascular phases of CEUS showed no significant differences between the hyperechoic group and iso-/hypoechoic group ($P>0.05$ for both readers, χ^2 test). Details of the grade of enhancement of benign and malignant FLLs on different vascular phases of CEUS were shown in Tables 3 and 4.

Table 4 Enhancement level of malignant focal liver lesions on different vascular phases

Baseline US	Reader	Arterial phase			Portal phase			Late phase		
		Hyper	Iso	Hypo	Hyper	Iso	Hypo	Hyper	Iso	Hypo
Hyperechoic	1	38	2	2	2	4	36	1	2	39
	2	39	2	1	2	3	37	1	1	40
Isoechoic	1	17	5	1	0	4	19	0	3	20
	2	17	5	1	0	4	19	0	2	21
Hypoechoic	1	111	9	1	3	29	89	2	9	110
	2	112	8	1	3	27	91	2	10	109
P	1	0.060			0.275			0.431		
	2	0.069			0.203			0.686		

With regard to differentiation of malignant FLLs from benign ones by using the rule of contrast washout in the portal and late phases of CEUS, the numbers of lesions with an allocated confidence level in terms of definitely benign, probably benign, indeterminate, probably malignant, and definitely malignant were 56 (49.1%), 13 (11.4%), 1 (0.9%), 10 (8.8%), and 34 (29.8%) for hyperechoic FLLs, and 94 (34.3%), 27 (9.9%), 8 (2.9%), 24 (8.8%), and 121 (44.2%) for iso- and hypoechoic FLLs in reader 1. The corresponding numbers in reader 2 were 56 (49.1%), 12 (10.5%), 2 (1.8%), 8 (7.0%), and 36 (31.6%) for hyperechoic FLLs, and 102 (37.2%), 15 (5.5%), 12 (4.4%), 23 (8.4%), and 122 (44.5%) for iso- and hypoechoic ones, respectively. The diagnostic performances of CEUS in differentiation of malignant FLLs from benign ones for hyperechoic FLLs in terms of Az were 0.987 (reader 1) and 0.981 (reader 2), and 0.987 (reader 1) and 0.984 (reader 2) for iso- and hypoechoic FLLs, respectively (Fig. 1). The interobserver agreement was very good, with κ=0.851 for hyperechoic FLLs and κ=0.812 for iso- and hypoechoic ones. The diagnostic performance of CEUS on FLLs with different echogenicity on baseline gray-scale US in terms of sensitivity, specificity, PPV, NPV, and accuracy was 87.0–95.9%, 93.1–100%, 88.6–100%, 70.0–97.1% and 90.0–95.1%, respectively.

Correct characterizations were made in 93.0% (106/114) hyperechoic lesions and 91.6% (251/274) iso- and hypoechoic lesions by reader 1, and 93.9% (107/114) and 90.5%

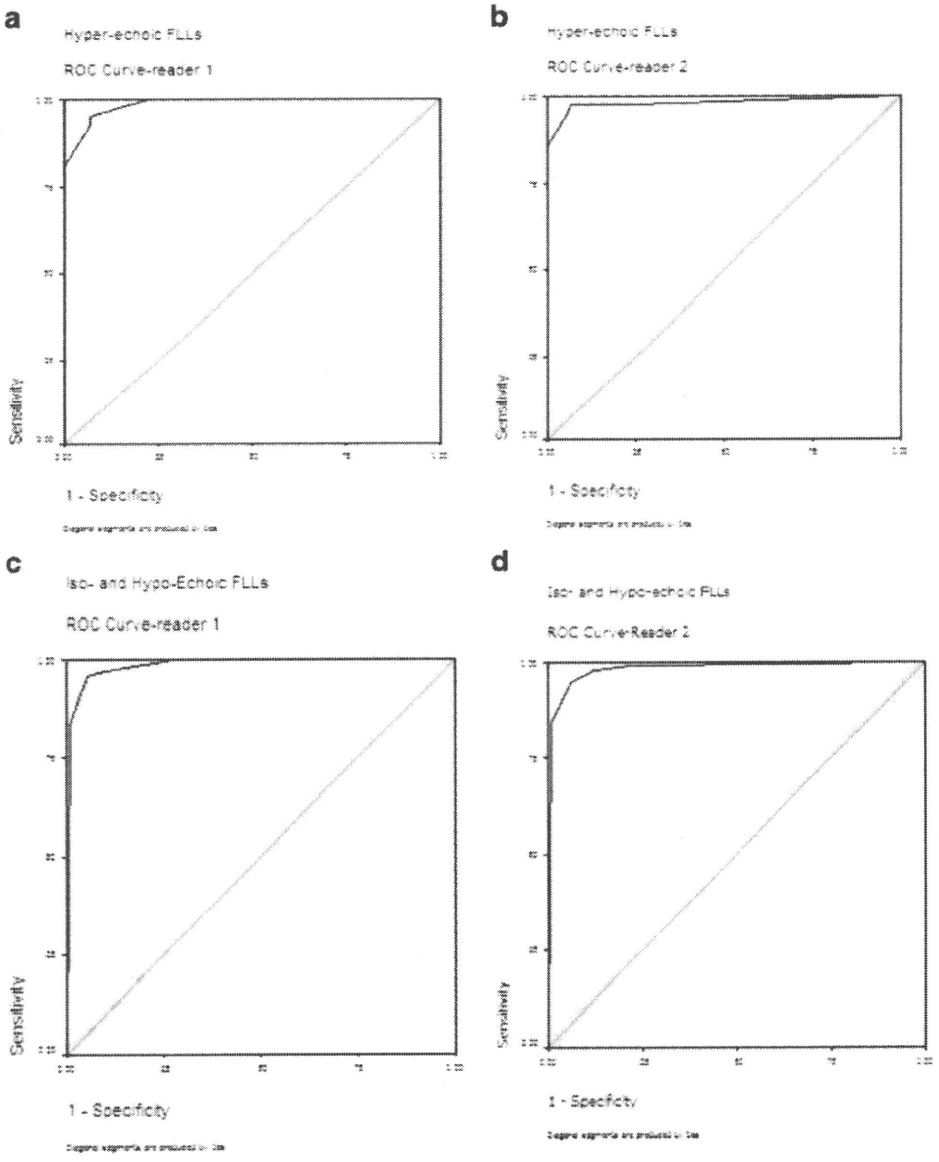

Fig. 1a–d Diagnostic performance of CEUS on small focal liver lesions with different echogenicity on baseline gray-scale US. ROC curves are plotted to discriminate malignant from benign focal liver lesions. **a** performance of reader 1 for hyperechoic lesions (Az: 0.987, range 0.973–1.001); **b** performance of reader 2 for hyperechoic lesions (Az: 0.981, range 0.950–1.012); **c** performance of reader 1 for iso- and hypoechoic lesions (Az: 0.987, range 0.975–0.998); **d** performance of reader 2 for iso- and hypoechoic lesions (Az: 0.984, range 0.970–0.998)

(248/274) by reader 2, respectively (P=0.974, χ^2 test). Both readers made wrong diagnoses in the same 24 lesions, including 6 inflammatory pseudotumors (hyperechoic in 1, hypoechoic in 5), 4 HCCs (hyperechoic in 1, isoechoic in 1 and hypoechoic in 2), 3 MRNs (hypoechoic in 1, hyperechoic in 2), 3 ICCs (both hypoechoic), 2 FNHs (both hypoechoic), 2 dysplastic nodules (both hypoechoic), 1 abscess (hypoechoic), 1 MLC from renal carcinoma (hyperechoic), 1 lymphoma (hypoechoic) and 1 focal fatty sparing (hypoechoic).

Discussion

Conventional gray-scale US is the most convenient imaging modality to detect and characterize FLLs during clinical practice. The newly developed CEUS techniques, which follow upon the merits of convenience and economy of conventional gray-scale US, were widely used to characterize FLLs by demonstrating accurate information of vascularity in lesions. As expected, satisfactory performance on characterization of FLLs with real-time CEUS and second-generation UCA has been reported in many studies [1–5].

Contrast-specific imaging techniques mainly use two different mechanisms to stimulate the nonlinear response of UCA microbubbles, one is oscillating the microbubbles at low acoustic pressure and the other is destroying the microbubbles under high acoustic pressure [1, 7, 11]. Although high MI (>0.5) techniques can show very strong stimulation of acoustic emission signals and produce bright transient signal enhancement, the weaknesses are that the harmonic response from tissue increases with acoustic pressure and enhancement can only been imaged intermittently. Low MI (<0.2) techniques can achieve the most of non-linear response from the second generation of UCA microbubbles and the least response from tissues in a real-time mode. However, harmonic frequencies from tissue still cannot be completely avoided during the imaging process, which may degrade the imaging quality of CEUS [7–9]. Different kinds of tissues show variable abilities to generate harmonic signals when exposed to US; this is particularly true in deep or fat tissues, which usually present a particular challenge to CEUS because bubble-to-tissue contrast is seriously decreased due to insufficient depression of the echoes from these tissues. For those FLLs which are hyperechoic on baseline gray-scale US, especially due to containing fat tissues, the enhancement caused by the contrast agent is added to the baseline echogenicity and can produce an erroneous interpretation of the degree of enhancement of those lesions [9].

In the present study, the grade of enhancement of benign FLLs on arterial phase and malignant FLLs during all the vascular phases of CEUS showed no significant differences between the hyper- and iso/hypoechoic lesions according to the echogenicity on baseline gray-scale US. The hyperechoic FLLs in the present study were mainly composed of 30 HCCs, 45 hemangiomas, 11 MLCs, and

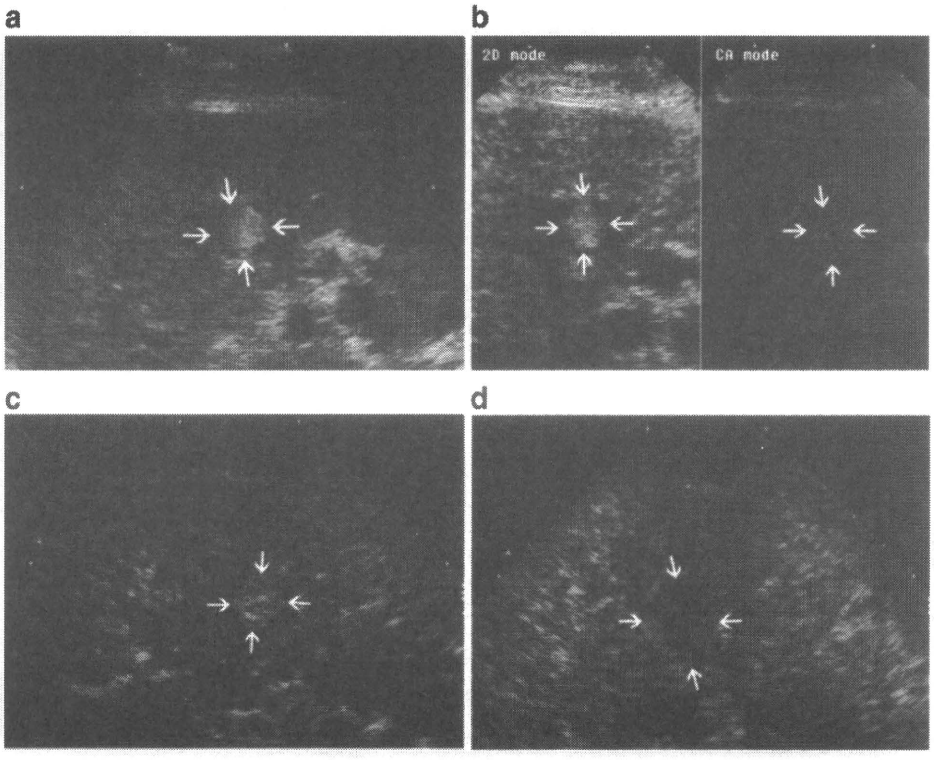

Fig. 2a–d HCC in a 57-year-old man. **a** Baseline sonography shows a hyperechoic lesion (*arrows*) sized 1.5 cm in diameter in segment 4. **b** CEUS image with CPS technique obtained before contrast agent administration shows not enough suppression of baseline information (CA mode, right side of the image, *arrows*). **c** CEUS image obtained 18 s after contrast agent administration shows homogeneous hyperenhancement of the lesion (*arrows*). **d** CEUS image obtained 78 s after contrast agent administration shows homogeneous hypoenhancement of the lesion (*arrows*)

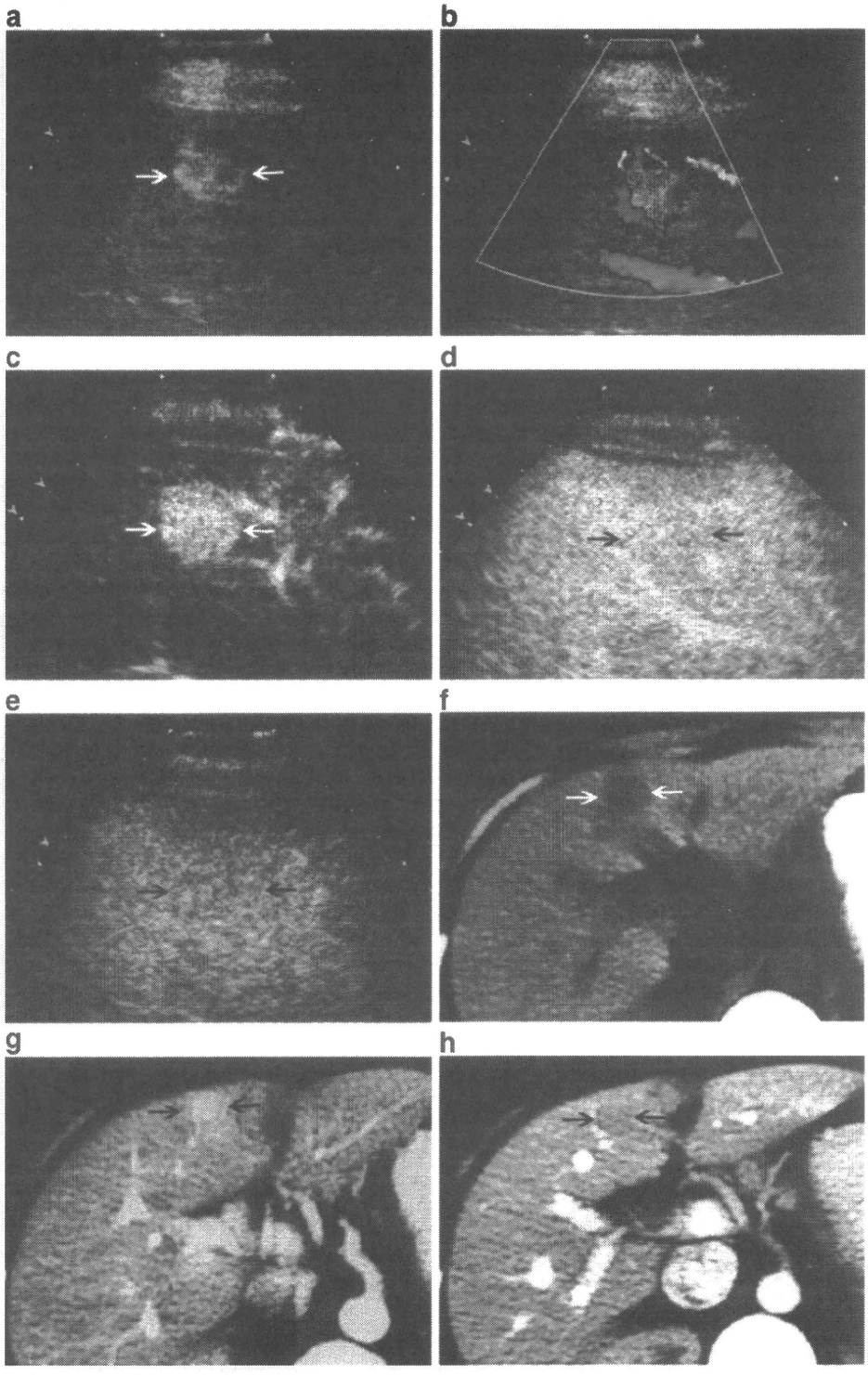

Fig. 3a–h Angiomyolipoma in a 34-year-old woman. **a** Baseline sonography shows a hyperechoic lesion (*arrows*) sized 2.5 cm in diameter in segment 4. **b** Color Doppler image shows peripheral vascularity. **c** CEUS image with CPS technique obtained 16 s after contrast agent administration shows homogeneous hyperenhancement of the lesion (*arrows*). **d** CEUS image obtained 57 s after contrast agent administration shows homogeneous isoenhancement of the lesion (*arrows*). **e** CEUS image obtained 180 s after contrast agent administration shows homogeneous isoenhancement of the lesion (*arrows*). **f** CT plain US study shows a low attenuation lesion in segment 4 (*arrows*). **g** Arterial phase of contrast-enhanced CT shows hyperenhancement of the lesion (*arrows*). **h** Portal phase of contrast-enhanced CT shows isoenhancement of the lesion (*arrows*)

18 MRNs. Except for some of the HCC and MRN lesions, it seems the majority of the hyperechoic lesions lack fat tissues [12, 13] (Fig. 2). The only angiomyolipoma lesion which surely contains fat tissues showed homogeneous hyperenhancement in the arterial phase and isoenhancement in the portal and late phases, and was coordinate with contrast enhancement on CT (Fig. 3). We believe that high MI techniques may be helpful to eliminate the influence of baseline echogenicity by displaying bright high-resolution color signals superimposed on a conventional B-mode image when evaluating the blood supply of hyperechoic FLLs containing fat tissues.

D'Onofrio et al. [6] studied 88 hypoechoic liver lesions with harmonic contrast-specific imaging and second-generation UCA microbubbles. According to the results obtained during the sinusoidal phase, they found that CEUS distinguished malignant from benign hypoechoic liver lesions with an accuracy of 95%. According to the specific enhancement pattern of the entire vascular phase, they correctly characterized 81% hypoechoic benign lesions and 88% malignant lesions. Our results showed that the diagnostic capability of CEUS did not interfere with echogenicity of FLLs on baseline gray-scale US for discrimination between malignant and benign lesions. The diagnostic performance of CEUS in terms of Az ranged from 0.981 to 0.987 for FLLs with different echogenicity on baseline gray-scale US, and a very good interobserver agreement was achieved in this study. The diagnostic accuracy of CEUS in differentiation between benign and malignant FLLs was in a range of 90–95% in the present study, which was coincident with the overall diagnostic accuracy of 85–95% reported in other studies [2, 3, 5, 6].

As to specific characterization of FLLs using CEUS, there was also no significant difference between FLLs with different echogenicity on baseline gray-scale US in the present study. The correctly characterized lesions were over 93% for hyperechoic FLLs, and over 90% for both iso- and hypoechoic FLLs. Since the enhancement patterns of several kinds of FLLs on CEUS are very characteristic and well-known for the radiologists, the specific diagnoses of HCC, FNH, hemangiomas, focal fatty infiltration or sparing by using CEUS show very high accuracy [1–5]. In the present study, both readers only made wrong diagnoses in less than 3% of FNHs, HCCs and focal fatty sparing lesions, while 100% of inflammatory pseudotumors and lymphoma, 75% of ICCs, 67% of dysplastic nodules, 33% of abscess, 7% of MRNs were misdiagnosed. Among the FLLs misdiagnosed by both readers, there were 5 hyperechoic lesions, 1 isoechoic lesion and 18 hypoechoic lesions. As described in previous studies, the CEUS findings of an inflammatory pseudotumor were nonspecific and easily mimic malignant FLLs, and biopsy is strongly recommended to confirm the diagnosis and avoid unnecessary surgery [14, 15]. ICC mainly shows irregular peripheral rim-like or heterogeneous hyperenhancement in the arterial phase and hypoenhancement in the portal and late phases. Although we reported that about 94% of ICCs were correctly characterized by combining the baseline and CEUS findings [16], there is a lack of specific imaging findings to confirm the diagnosis of small ICCs, as in the present study. The diagnoses of MRN and dysplastic nodules in the cirrhotic liver were reported to be extremely difficult by a variety of noninvasive imaging modalities [17–19]. Again histopathological examination remains the only way to clarify the diagnosis of MRN and dysplastic nodule. Typical enhancement features of liver abscess on CEUS have been well depicted in previous series [1, 14, 20]. In the present study, one misdiagnosed liver abscess showed untypical appearance both on baseline US and CEUS. Because of the time-dependent imaging findings of hepatic abscess, it will be easy to misdiagnose it as malignant FLLs in the very early or late stage of abscess.

In conclusion, CEUS greatly improves the diagnostic ability of several kinds of FLLs such as HCC, FNH, hemangiomas and focal fatty change or sparing. The diagnostic performance of CEUS was not interfered by the echogenicity of lesion on baseline gray-scale US.

References

1. Claudon M, Cosgrove D, Albrecht T et al (2008) Guidelines and good clinical practice recommendations for contrast enhanced ultrasound (CEUS)—Update 2008. Ultraschall Med 29:28–44
2. Quaia E, Caliada F, Bertolotto M et al (2004) Characterization of focal liver lesions with contrast-specific US modes and a sulfur hexafluoride-filled microbubble contrast agent: diagnostic performance and confidence. Radiology 232:420–430
3. von Herbay A, Vogt C, Willers R, Häussinger D (2004) Real-time imaging with the sonographic contrast agent SonoVue: differentiation between benign and malignant hepatic lesions. J Ultrasound Med 23:1557–1568
4. Ding H, Wang WP, Huang BJ et al (2005) Imaging of focal liver lesions: low-mechanical-index real-time ultrasonography with SonoVue. J Ultrasound Med 24:285–297
5. Xu HX, Liu GJ, Lu MD et al (2006) Characterization of small focal liver lesions using real-time contrast-enhanced sonography: diagnostic performance analysis in 200 patients. J Ultrasound Med 25:349–361
6. D'Onofrio M, Rozzanigo U, Masinielli BM et al (2005) Hypoechoic focal liver lesions: characterization with contrast enhanced ultrasonography. J Clin Ultrasound 33:164–172
7. Solbiati L, Martegani A, Leen E, Correas JM, Burns PN, Becker D (2003) Contrast-enhanced ultrasound of liver diseases. Springer, Milan
8. Cosgrove DO, Blomley MJ, Eckersley RJ et al (2002) Innovative contrast specific imaging with ultrasound. Electromedica 70:147–150

9. Wilson SR, Kim TK, Jang HJ, Burns PN (2007) Enhancement patterns of focal liver masses: discordance between contrast-enhanced sonography and contrast-enhanced CT and MRI. AJR Am J Roentgenol 189:W7–W12
10. Llovet JM, Fuster J, Bruix J, Barcelona-Clinic Liver Cancer Group (2004) The Barcelona approach: diagnosis, staging and treatment of hepatocellular carcinoma. Liver Transpl 10:S115–S120
11. de Jong N, Bouakaz A, Frinking P (2002) Basic acoustic properties of microbubbles. Echocardiography 19:229–240
12. Ishak KG, Goodman ZD, Stocker JT (2001) Tumors of the liver and intrahepatic bile ducts. Atlas of Tumor Pathology, Armed Forces Institute of Pathology, Washington D.C.
13. Choi BI, Takayasu K, Han MC (1993) Small hepatocellular carcinomas and associated nodular lesions of the liver: pathology, pathogenesis, and imaging findings. AJR Am J Roentgenol 160:1177–1187
14. Liu GJ, Lu MD, Xu HX et al (2008) Real-time contrast-enhanced ultrasound imaging of infected focal liver lesions. J Ultrasound Med 27:657–666
15. Yoon KH, Ha HK, Lee JS et al (1999) Inflammatory pseudotumor of the liver in patients with recurrent pyogenic cholangitis: CT-histopathologic correlation. Radiology 211:373–379
16. Xu HX, Lu MD, Liu GJ et al (2006) Imaging of peripheral cholangiocarcinoma with low-mechanical index contrast-enhanced sonography and SonoVue: initial experience. J Ultrasound Med 25:23–33
17. Rode A, Bancel B, Douek P et al (2001) Small nodule detection in cirrhotic livers: evaluation with US, spiral CT, and MRI and correlation with pathologic examination of explanted liver. J Comput Assist Tomogr 25:327–336
18. Gritzmann N (2003) Small hepatocellular carcinomas in patients with liver cirrhosis: potentials and limitations of contrast-enhanced power Doppler sonography. Eur J Gastroenterol Hepatol 15:881–883
19. Lim JH, Kim MJ, Park CK, Kang SS, Lee WJ, Lim HK (2004) Dysplastic nodules in liver cirrhosis: detection with triple phase helical dynamic CT. Br J Radiol 77:911–916
20. Catalano O, Sandomenico F, Raso MM, Siani A (2004) Low mechanical index contrast-enhanced sonographic findings of pyogenic hepatic abscess. AJR Am J Roentgenol 182:447–450

Efficacy of Perflubutane Microbubble–Enhanced Ultrasound in the Characterization and Detection of Focal Liver Lesions: Phase 3 Multicenter Clinical Trial

Fuminori Moriyasu[1]
Kouichi Itoh[2,3]

OBJECTIVE. The purpose of this study was to assess the efficacy and safety of contrast-enhanced ultrasound performed with perflubutane microbubbles in comparison with unenhanced ultrasound and dynamic CT in the characterization of focal liver lesions during the vascular phase of imaging and in the detection of lesions during the Kupffer phase.

SUBJECTS AND METHODS. A total of 196 patients were enrolled at 15 centers in Japan. Vascular phase images were obtained before contrast injection until 1 minute after injection. Kupffer phase images were obtained 10 minutes after injection. Dual-phase CT was performed as determined by standard clinical practice at each center. Unenhanced ultrasound, contrast-enhanced ultrasound, and CT images were read by blinded reviewers, and the results they reached regarding characterization and detection were compared with reference standard findings made by onsite investigators. The safety observation period was 72 hours after contrast administration.

RESULTS. Among the 190 patients included in the characterization analysis, the accuracy of contrast-enhanced ultrasound (88.9%) was significantly greater than that of unenhanced ultrasound (68.4%) and dynamic CT (80.5%) ($p < 0.001$ and $p = 0.008$). Among the 191 patients in the detection analysis, the efficacy of contrast-enhanced ultrasound in detection of lesions was significantly higher than that of unenhanced ultrasound and dynamic CT ($p < 0.001$ and $p = 0.008$), predominantly because more metastatic lesions were detected (both $p < 0.001$). In particular, contrast-enhanced ultrasound was superior to dynamic CT in the detection of metastatic lesions measuring 1 cm or smaller. The incidence of adverse events was 49.2% and that of adverse drug reactions was 10.4%. All adverse drug reactions were mild.

CONCLUSION. Compared with unenhanced ultrasound and dynamic CT, contrast-enhanced ultrasound with perflubutane microbubbles improved diagnostic efficacy in both characterization and detection of focal liver lesions with no serious adverse drug reactions.

Keywords: characterization, detection, contrast-enhanced ultrasound, focal liver lesions, perflubutane

DOI:10.2214/AJR.08.1618

Received August 1, 2008; accepted after revision December 29, 2008.

Funding for this study was provided by Daiichi Pharmaceutical Company. Perflubutane microbubbles were provided by Amersham Health. Authors who were not employees of either sponsor controlled the inclusion of any data and information that might have presented a conflict of interest for employees of either sponsor.

[1]Department of Gastroenterology and Hepatology, Tokyo Medical University, 6-7-1 Nishishinjuku, Shinjuku-ku, Tokyo 160-0023 Japan. Address correspondence to F. Moriyasu (moriyasu@tokyo-med.ac.jp).

[2]Department of Clinical Laboratory Medicine, Jichi Medical School, Tochigi, Japan.

[3]Present address: Hitachiomiya Saiseikai Hospital, Ibaragi, Japan.

AJR 2009; 193:86–95

0361–803X/09/1931–86

Contrast agents for sonography are principally gas-encapsulated microbubbles. Successful efforts have been made to produce microbubbles that are sufficiently small and stable to pass into the systemic circulation after IV administration [1, 2]. Initially, the efficacy of commercially available air-based microbubble agents was limited because the bubbles were easily destroyed by ultrasound exposure [3–5]. With modification of the composition of the microbubble shell and use of a lower-solubility substance such as a perfluorochemical instead of gas, stability and resistance to pressure were improved [6, 7]. The critical improvement has been development of microbubble-specific imaging techniques that work at a low enough mechanical index to minimize destruction of microbubbles [8–10]. The development of perfluorochemical gas–encapsulated microbubbles and high-frame-rate real-time scanning for contrast-enhanced ultrasound (CEUS) enabled the study of early arterial events, leading to accurate diagnosis of liver lesions owing to visualization of the tumor vasculature and specific enhancement patterns [11–13].

The perflubutane microbubbles used in this study are perfluorochemical agents consisting of microbubbles of perfluorobutane (C_4F_{10}) stabilized by a monomolecular membrane of hydrogenated egg phosphatidyl serine [14]. When the liver is imaged in the phase-modulation harmonic mode, CEUS with perflubutane microbubbles has two phases of contrast enhancement: vascular and Kupffer phase. Vascular phase images are acquired soon after IV contrast injection and can be used to

characterize selected lesions on the basis of the dynamics of contrast enhancement (e.g., arterial and portal venous), morphologic features of the tumor vasculature, and tumor perfusion [15]. Unlike contrast-enhanced Doppler imaging, CEUS in the phase-modulation harmonic mode is expected to depict microvessels because the mode does not cause the blooming that often occurs in Doppler imaging.

Perflubutane microbubbles are taken up by Kupffer cells in the reticuloendothelial system of the liver, and this phenomenon allows parenchyma-specific imaging of the liver [16–18]. Parenchyma-specific imaging, called Kupffer phase imaging, is typically performed 10 minutes after contrast injection, at which time the normal hepatic parenchyma is enhanced, and malignant lesions that contain few or no Kupffer cells are clearly delineated as contrast defects [15, 19]. Therefore, it is conceivable that Kupffer phase imaging can be used to detect focal liver lesions. The diagnostic performance of microbubble agents that can be used for both the vascular and parenchyma-specific, or Kupffer, phases of hepatic ultrasound has not, to our knowledge, been evaluated in a controlled clinical study. The purpose of this prospective open-label multicenter phase 3 study was to assess the efficacy and safety of CEUS with perflubutane microbubbles in the characterization and detection of focal liver lesions in the vascular and Kupffer phases of imaging, respectively, in comparison with unenhanced ultrasound and dynamic CT (DCT).

Subjects and Methods

Patient Population

Before initiation, this study was approved by the institutional review boards at each of the 15 participating institutions. All patients provided written informed consent before entering the study. The subjects were patients who had at least one untreated focal liver lesion confirmed with a previous diagnostic study (e.g., DCT, contrast-enhanced MRI, angiography, pathologic examination). Inclusion criteria were the presence of a hepatic mass or lesion confirmed at DCT within the past month (past 3 months for benign tumors), fewer than 10 known lesions, and being a man or woman 20–80 years old.

The exclusion criteria were terminal clinical condition and life expectancy of 3 months or less; previous administration of perflubutane microbubbles; ongoing transcatheter chemotherapy or radiation therapy; current or within the past 180 days participation in another clinical study; pregnancy, possible pregnancy, or lactation; history of allergy to eggs or egg products; surgical procedure or liver biopsy within 24 hours before administration of perflubutane microbubbles; administration or scheduled administration of another contrast agent within 24 hours before or after administration of perflubutane microbubbles; difficulty in recognition of a target lesion previously determined with DCT or difficulty with a scan of the whole liver with unenhanced ultrasound owing to poor baseline image quality; and mass or lesion size 10 cm or greater.

Among 196 patients enrolled from April 2002 to March 2003, three patients were excluded from the study: Two did not receive perflubutane microbubbles and one had a good clinical practices violation. Of the 193 patients eligible for safety evaluation, 130 were men and 63 were women. The mean age was 63 years (range, 23–80 years). Among the 193 patients eligible to participate in the safety evaluation, 190 patients were eligible for evaluation of the efficacy of vascular phase imaging and 191 for evaluation of the efficacy of Kupffer phase imaging. One patient was excluded from the efficacy evaluation for not meeting the study recruitment criteria. In addition, two patients from vascular and one patient from the Kupffer phase imaging were excluded because they missed the video recording. The number of patients eligible for vascular phase imaging included 121 with hepatocellular carcinoma (HCC), 38 with metastatic lesions, 17 with hemangiomas, nine with other benign lesions, and five with other malignant lesions. One additional patient with a benign lesion was included in the evaluation of Kupffer phase imaging.

Contrast Agent

Perflubutane microbubbles (Sonazoid, GE Healthcare) is a lyophilized preparation reconstituted for injection and contains 16 μL of perflubutane microbubbles in one vial. The contents of each vial were resuspended in 2 mL of water for injection. Each patient received a single injection of 0.12 μL/kg of microbubbles (0.015 mL/kg of the reconstituted suspension) into a forearm vein followed by a 10-mL saline flush.

Ultrasound

All ultrasound scanners (Aplio, Toshiba Medical Systems; Elegra, Siemens Healthcare; EUB 8500, Hitachi; HDI 5000, Phillips Healthcare; Logiq 7, GE Healthcare; Sequoia 512, Siemens Healthcare) were equipped with broadband curved-array transducers adapted for contrast imaging. Ultrasound was performed before and after enrollment. Unenhanced ultrasound performed before enrollment was used as a reference standard and to assess whether the subject met the inclusion criteria and fulfilled none of the exclusion criteria. Ultrasound imaging was performed after enrollment to compare the efficacy of CEUS with perfluorobutane microbubbles. In each patient, one lesion of interest, which had not been treated and was confirmed with DCT, was selected for vascular phase imaging for lesion characterization. The whole liver was scanned in the Kupffer phase for lesion detection. Unenhanced ultrasound images corresponding to both the vascular and the Kupffer phase images also were acquired for assessment by the blinded reviewers. All ultrasound images were acquired by onsite investigators according to the following imaging conditions and were recorded on S-VHS videotape for review by the blinded readers.

Unenhanced ultrasound (baseline image)—The lesion of interest was imaged for 15 seconds with each of the following techniques: fundamental B mode, tissue harmonic B mode, color Doppler, and power Doppler. Afterward, the whole liver was scanned, first in fundamental B mode and then in tissue harmonic B-mode.

CEUS—Phase-modulation harmonic mode was used for both vascular and Kupffer phase imaging (mechanical index, 0.3–0.5; frame rate, 8–10 frames/s; transmitting frequency, 1.5–2 MHz). The focus was set below the lesion of interest for vascular phase imaging and at 4–8 cm for the left lobe and 8–10 cm for the right lobe for Kupffer phase imaging. The lesion of interest was imaged from 15 seconds before injection to 1 minute after injection (vascular phase imaging). No further scanning was performed until the Kupffer phase imaging, which was begun 10 minutes after injection. The whole liver was scanned twice with the same protocol as for unenhanced ultrasound.

Dynamic CT

Dual-phase dynamic contrast-enhanced studies were performed with helical CT or MDCT. Twelve centers used MDCT and three centers used helical CT. The imaging conditions were not standardized for this study because DCT was performed before enrollment but had been optimized by the respective centers with a mean slice thickness of 6.9 ± 2.0 (SD) mm (range, 2–10 mm). DCT was performed within the month before enrollment for malignant tumors and within 3 months before enrollment for benign tumors. These images were provided for review by the blinded readers.

Reference Standard

The reference standard procedures, which had been performed by onsite investigators before study enrollment, included diagnostic imaging

with unenhanced ultrasound and DCT, acquisition of relevant clinical information such as history or existing disorder, and assessment of clinical and biochemical biomarkers. If necessary, dynamic MRI, angiography, or pathologic examination was added.

For characterization, the disease diagnosis was changed when it was believed it would be changed after CEUS and it was confirmed during treatment, or it was changed in the process of treatment during this study period. The disease diagnosis was changed in eight cases, including three cases influenced by CEUS findings. Seven of the eight cases were confirmed at histologic examination of specimens obtained at biopsy or surgery, and one case was confirmed in follow-up. For detection, the number and size of the lesions were recorded by onsite investigators on the basis of findings at unenhanced ultrasound, DCT, or other procedure before enrollment and were used as the reference standards. Patients with newly detected lesions visible only with CEUS underwent follow-up by onsite investigators for 3 months. To confirm whether a lesion was a true lesion, onsite investigators used techniques such as DCT, contrast-enhanced MRI, angiography, biopsy, surgery, or a combination of these procedures, except for unenhanced ultrasound and CEUS.

Image Reading

Two readings were performed: an unblinded reading by onsite investigators who had access to all clinical and imaging information and an offsite reading by blinded reviewers. Three blinded reviewers for ultrasound and another three blinded reviewers for DCT were selected from specialists in the field who were independent of the onsite investigators and the coordinating investigator. Unenhanced ultrasound and CEUS videotapes for readings by blinded reviewers were made after enrollment, whereas DCT images were obtained before enrollment. Patient and site identification data were removed from the ultrasound videotapes and CT images. The ultrasound videotapes and CT images then were randomized into three equal portions. Each reader reviewed one third of the total number of cases.

Before evaluation, the three reviewers received training to maintain consistency in the evaluation criteria. For confirmation of reliability after the training, each reader independently evaluated ultrasound videotapes and CT images from 20 cases that had been randomized and from which identifying information was removed. In the characterization assessment, the rates of complete agreement on unenhanced ultrasound, CEUS, and DCT findings among the three reviewers were 85%, 90%, and 90%. In detection assessment, the rates were 95%, 90%, and 90%. These percentages suggest that interobserver reliability was ensured.

The blinded reviewers assessed the images without clinical information and without knowledge of the results of the onsite evaluation. For characterization with ultrasound, the blinded reviewers interpreted unenhanced ultrasound videotapes depicting only the lesion of interest in each patient separately from tapes containing the vascular phase of CEUS. For detection with ultrasound, the reviewers interpreted unenhanced ultrasound videotapes containing only whole liver scans for each patient separately from those containing the Kupffer phase of CEUS. For CT, the reviewers read CT images containing only slices depicting the lesion of interest for characterization. CT images of all liver slices were used for detection.

In the characterization assessments, the reviewers classified their diagnoses into five categories: HCC, hepatic metastasis, hemangioma, other benign lesion, and other malignant lesion. In addition, the reviewers of ultrasound images reported their degree of confidence in their diagnoses as definite, probable, or suspect. In detection, the reviewers of both ultrasound and DCT images recorded the location and size of the lesions.

Efficacy Evaluation

The results of the assessments by the blinded reviewers with each technique (unenhanced ultrasound, CEUS, and DCT) were compared with reference standard findings by the onsite investigators. For evaluation of characterization efficacy, the rates of correct diagnoses for the various lesion types were assessed and compared for unenhanced ultrasound, CEUS, and DCT. Sensitivity and specificity were calculated for correct classification of lesions as malignant or benign. Degree of confidence in the diagnosis was compared between unenhanced ultrasound and CEUS. For evaluation of detection efficacy, the numbers of patients in whom the number of lesions detected by blinded reviewers was less than, equal to, or more than that detected with the reference standard were calculated for unenhanced ultrasound, CEUS, and DCT and compared. In addition, the numbers of lesions detected by blinded reviewers were used to compare efficacy between methods. Efficacy in terms of detection of different types of lesions and of detection of lesions in various size categories was evaluated in a similar manner. In the cases of patients whose treatment strategy was changed on the basis of information from CEUS, the reasons for doing so were recorded.

Safety Evaluation

Safety was evaluated by the onsite investigators. Clinical chemistry variables and vital signs were assessed immediately before and within 24 hours after injection. Patients were observed for adverse events for 72 hours after injection, and the severity and causes of the events were assessed. Serious adverse events were observed for 7 days. Severity criteria were as follows: mild, temporary and easily tolerable; moderate, interfering with normal activities; and severe, completely preventing normal activities.

Statistical Analysis

For assessment of characterization efficacy, the McNemar test was used to compare the rates of correct diagnosis of lesions for unenhanced ultrasound, CEUS, and DCT. For assessment of detection efficacy, Wilcoxon's signed rank test was used to compare the lesion detection rates obtained with unenhanced ultrasound, CEUS, and DCT. For all tests, $p < 0.05$ was considered to indicate a statistically significant difference. A statistical software package (SAS version 8.2, SAS) was used for the statistical analyses.

Results

Characterization

Different types of focal lesions had different patterns of enhancement on vascular phase images. Typical enhancement patterns of HCC, metastasis, and hemangioma on CEUS and DCT images are shown in Figures 1–3. In all cases, CEUS images were adequate for assessment. In no case was lesion contrast missing owing to artifacts from the microbubbles.

As shown in Table 1, the overall rate of correct diagnosis of lesions by the blinded reviewers significantly improved from 68.4% for unenhanced ultrasound to 88.9% for CEUS ($p < 0.001$). In addition, the overall rate of correct diagnosis with CEUS was significantly higher than that with DCT (80.5%) ($p = 0.008$). In classification of the lesions into the five types, the rates of correct diagnosis of HCC, metastasis, and hemangioma were significantly higher for CEUS than for unenhanced ultrasound ($p < 0.001$, $p = 0.002$, and $p = 0.025$). In particular, all 17 cases of hemangioma were correctly diagnosed with CEUS (100%). The performance of CEUS in the correct diagnosis of metastasis was superior to that of DCT, but no significant differences were evident for other types of lesions.

In terms of correct classification of lesions as malignant or benign, the overall accuracy and sensitivity significantly improved from 86.3% and 89.0% for unenhanced ultrasound to 97.4% and 98.8% for CEUS (both $p <$ 0.001) (Table 2). In contrast, no significant

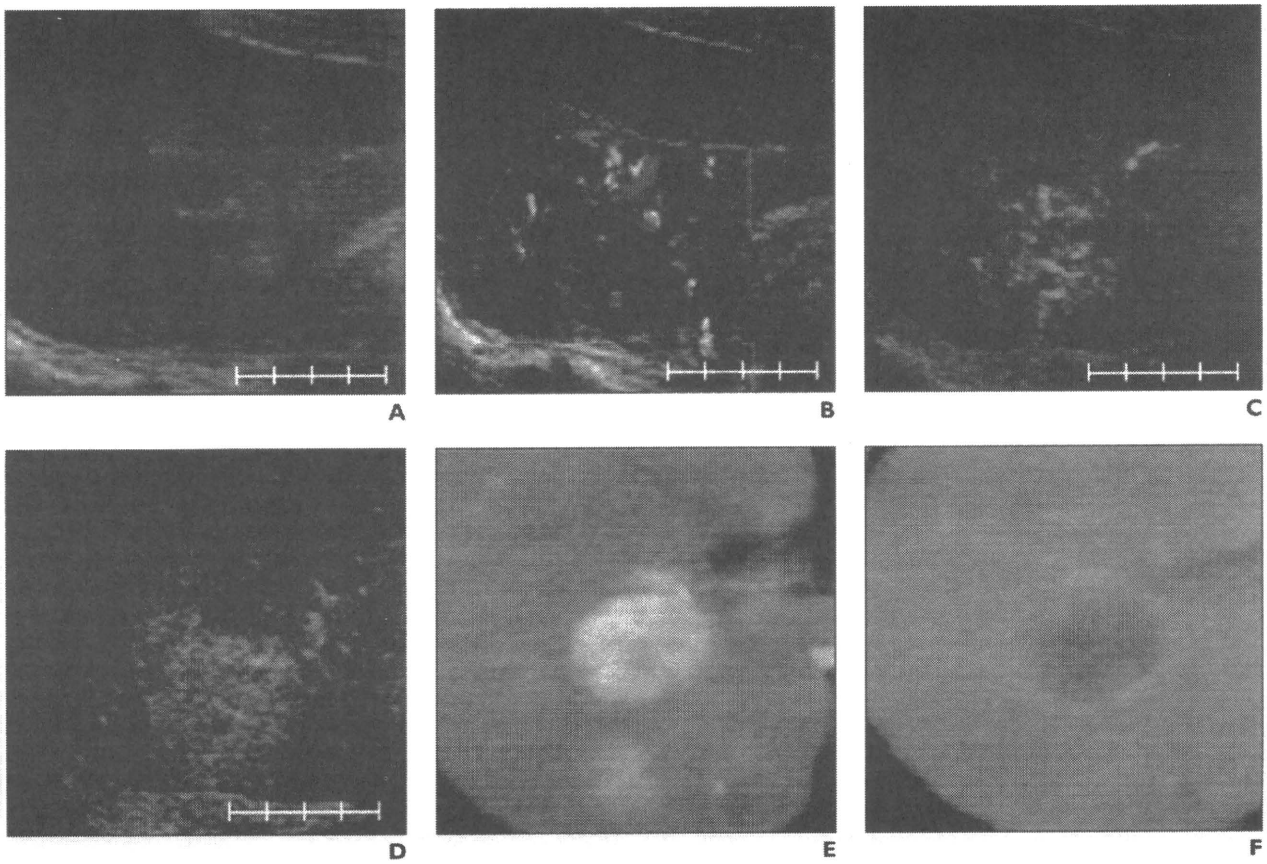

Fig. 1—75-year-old man with hepatocellular carcinoma. Scale bar = 4 cm.
A, B-mode ultrasound image shows mosaic speckle pattern in tumor.
B, Color Doppler ultrasound image shows increased vascularity in tumor.
C, Vascular phase perflubutane-enhanced ultrasound image shows fine tumor vessels.
D, Late vascular phase perflubutane-enhanced ultrasound image shows homogeneously enhanced perfusion in tumor 20 seconds after contrast injection.
E, Arterial phase dynamic CT image shows heterogeneous staining of tumor.
F, Portal venous phase dynamic CT image shows low-attenuation area with ringlike enhancement.

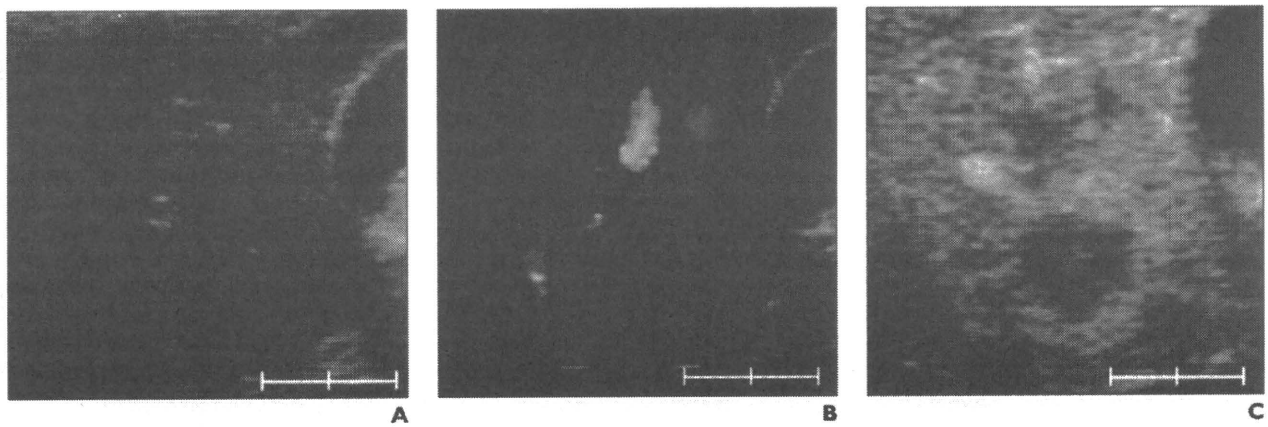

Fig. 2—59-year-old woman with liver metastasis. Scale bar = 2 cm.
A, B-mode ultrasound image shows hyperechoic tumor with thick halo and bull's-eye pattern.
B, Color Doppler ultrasound image shows little vascularity in tumor.
C, Vascular phase perflubutane-enhanced ultrasound image shows ring enhancement in peripheral portion of tumor.

(Fig. 2 continues on next page)

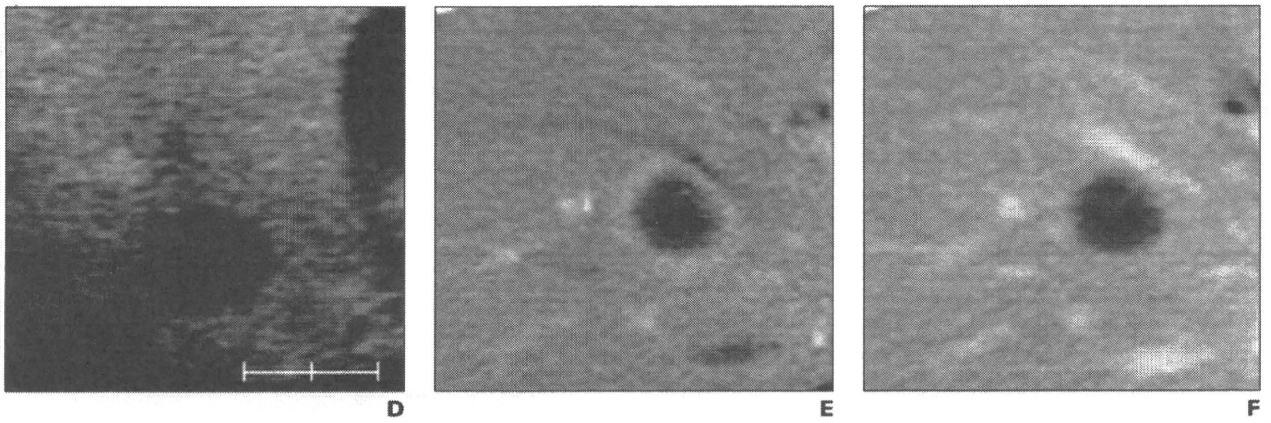

Fig. 2 (continued)—59-year-old woman with liver metastasis. Scale bar = 2 cm.
D, Late vascular phase perflubutane-enhanced ultrasound image shows clearly demarcated washout in tumor.
E, Arterial phase dynamic CT image shows ringlike enhancement in peripheral region of tumor.
F, Late phase dynamic CT image shows weak ring enhancement.

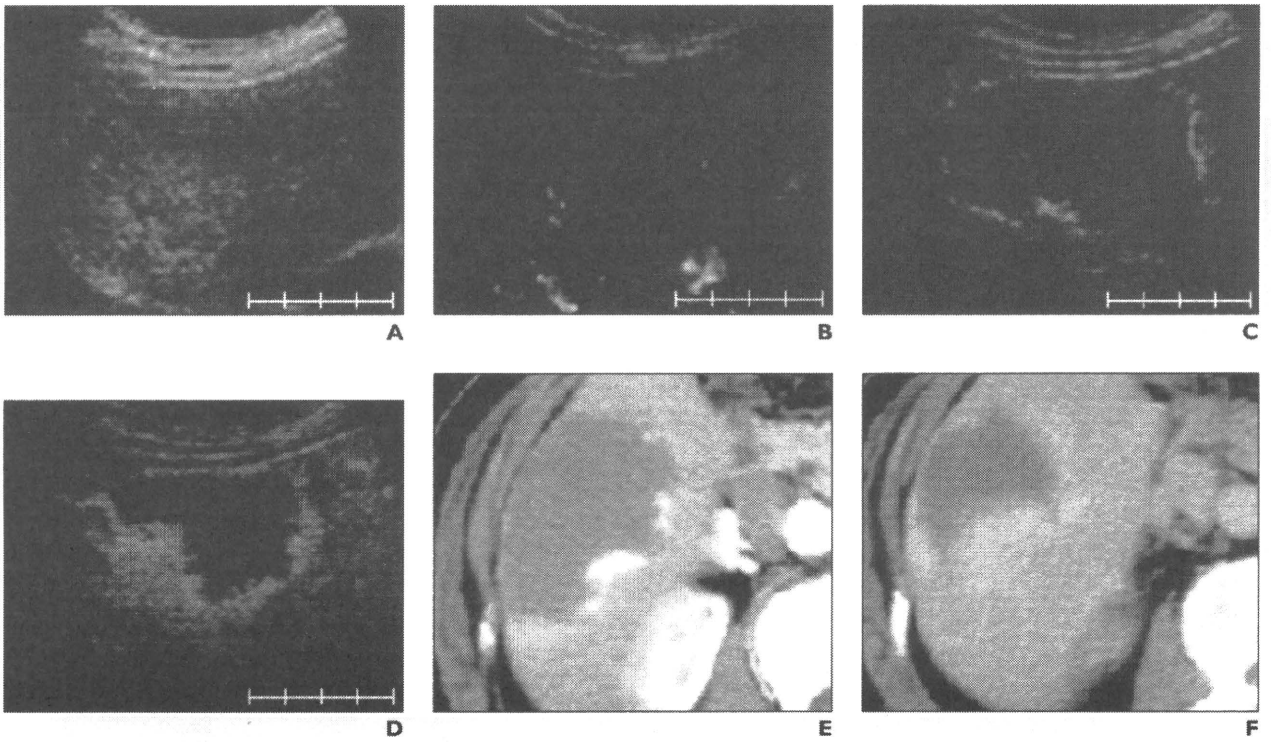

Fig. 3—59-year-old man with hemangioma. Scale bar = 4 cm.
A, B-mode ultrasound image shows hyperechoic elliptic mass with unclear delineation.
B, Color Doppler ultrasound image shows little inner vascular signal in tumor.
C, Vascular phase perflubutane-enhanced ultrasound image shows filling-in enhancement in peripheral portion of tumor.
D, Late vascular phase perflubutane-enhanced ultrasound image shows centripetal invasion of filling-in enhancement.
E, Arterial phase dynamic CT image shows filling-in enhancement.
F, Late phase dynamic CT image shows heterogeneous filling-in enhancement.

TABLE 1: Rate of Correct Diagnosis in Characterization of Focal Liver Lesions

Lesion Classification	Unenhanced Ultrasound	CEUS	DCT
Overall	68.4 (130/190)	88.9 (169/190)	80.5 (153/190)
Hepatocellular carcinoma	77.7 (94/121)	92.6 (112/121)	89.3 (108/121)
Metastasis	44.7 (17/38)	78.9 (30/38)	57.9 (22/38)
Hemangioma	70.6 (12/17)	100 (17/17)	94.1 (16/17)
Other benign lesion	44.4 (4/9)	66.7 (6/9)	33.3 (3/9)
Other malignant lesion	60.0 (3/5)	80.0 (4/5)	80.0 (4/5)

Note—Data are percentages. Numbers in parentheses are numbers of patients used for calculation of the percentages. McNemar test results were as follows: Overall—unenhanced ultrasound vs contrast-enhanced ultrasound (CEUS), $p < 0.001$; unenhanced ultrasound vs dynamic CT (DCT), $p = 0.006$; CEUS vs DCT, $p = 0.008$. HCC—unenhanced ultrasound vs CEUS, $p < 0.001$; unenhanced ultrasound vs DCT, $p = 0.016$. Metastasis—unenhanced ultrasound vs CEUS, $p = 0.002$; CEUS vs DCT, $p = 0.021$. Hemangioma—unenhanced ultrasound vs CEUS, $p = 0.025$; unenhanced ultrasound vs DCT, $p = 0.046$.

TABLE 2: Accuracy, Sensitivity, and Specificity in Characterization of Malignant and Benign Lesions

Characteristic	Unenhanced Ultrasound	CEUS	DCT
Overall accuracy	86.3 (164/190)	97.4 (185/190)	94.7 (180/190)
Sensitivity	89.0 (146/164)	98.8 (162/164)	95.7 (157/164)
Specificity	69.2 (18/26)	88.5 (23/26)	88.5 (23/26)

Note—Data are percentages. Numbers in parentheses are numbers of patients used for calculation of the percentages. Sensitivity and specificity are percentages of malignant and benign lesions correctly diagnosed. McNemar test results were as follows: Accuracy—contrast-enhanced ultrasound (CEUS) vs unenhanced ultrasound, $p < 0.001$; dynamic CT (DCT) vs unenhanced ultrasound, $p = 0.005$. Sensitivity—CEUS vs unenhanced ultrasound, $p < 0.001$; DCT vs unenhanced ultrasound, $p = 0.016$. Specificity—CEUS vs unenhanced ultrasound, $p = 0.096$; DCT vs unenhanced ultrasound, $p = 0.132$.

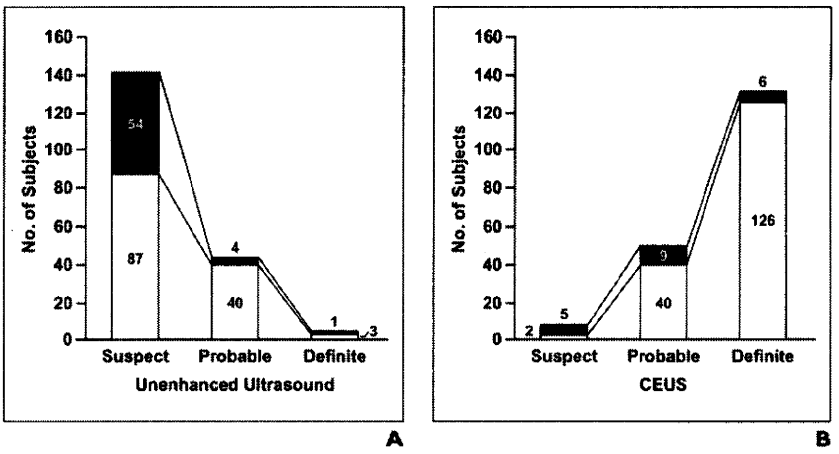

Fig. 4—Degree of confidence scored by blinded reviewers.
A and **B**, Graphs show degree of confidence in diagnoses made with unenhanced ultrasound (**A**) and contrast-enhanced ultrasound (CEUS) (**B**). Disagreement (*black*) indicates that diagnosis by blinded reviewers was not correct. Agreement (*white*) indicates diagnosis by blinded reviewers was correct.

differences in accuracy, sensitivity, or specificity were found between CEUS and DCT.

The level of diagnostic confidence scored by the blinded reviewers was compared between unenhanced ultrasound and CEUS (Fig. 4). The degree of confidence in diagnoses made with unenhanced ultrasound was scored definite in four of 189 cases (2.1%), and one of these diagnoses was incorrect. The number of diagnoses scored definite with CEUS increased to 132 of 189 (69.8%), and 126 of these diagnoses (95.5%) were correct.

Detection

Metastatic lesions were clearly depicted as contrast defects on CEUS Kupffer phase images (Fig. 5). Table 3 shows the number of patients in whom more, an equal number of, and fewer lesions were detected by the blinded reviewers than by the onsite readers using the reference standard. Using DCT, the blinded reviewers detected more or fewer lesions than were found with the reference standard in similar numbers of patients. Using CEUS, the blinded reviewers detected more lesions approximately twice as often as they detected fewer lesions. The percentages of patients in whom more lesions were detected by the blinded reviewers than were found with the reference standard were 31.9% (61 patients), 18.8% (36 patients), and 13.1% (25 patients) for CEUS, DCT, and unenhanced ultrasound (Table 3). The detection rate with CEUS was significantly higher than that with unenhanced ultrasound and DCT ($p < 0.001$ and $p = 0.008$).

The number of lesions detected with unenhanced ultrasound, CEUS, and DCT compared with the reference standard was determined for the five types of lesions, and the results are shown in Table 4. The number of lesion detected with CEUS was larger than that with unenhanced ultrasound and DCT. The number of lesions detected with CEUS (464 lesions) was larger than the number detected with the reference standard (375 lesions). It was particularly evident that the number of metastatic lesions detected with CEUS was significantly larger than the number detected with unenhanced ultrasound ($p < 0.001$) and the number detected with DCT ($p < 0.001$).

In classification of lesions according to size, the number of small lesions (≤ 1 cm) detected with CEUS was significantly larger than the number detected with unenhanced ultrasound ($p < 0.001$) and DCT ($p = 0.008$) (Fig. 6). Furthermore, in classification of metastatic lesions according to size, the number of lesions 1 cm in diameter or smaller

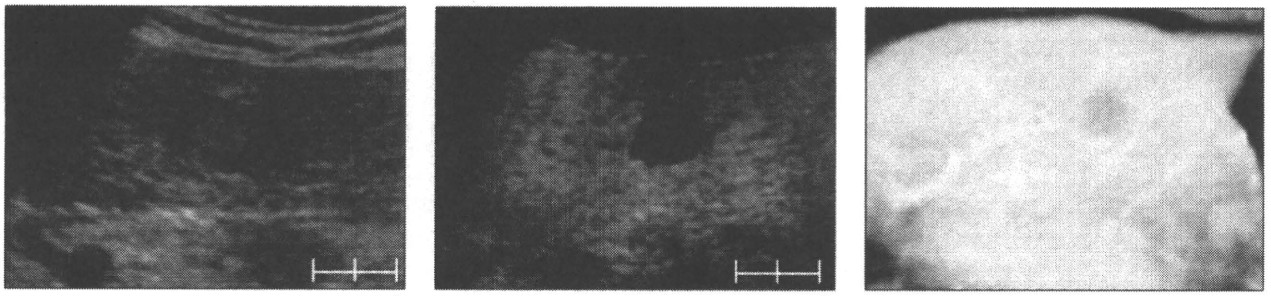

A B C

Fig. 5—59-year-old man with liver metastasis. Scale bar = 2 cm.
A, Ultrasound image shows heterogeneous hypoechoic mass in lateral segment of left lobe of liver.
B, Perflubutane-enhanced Kupffer phase ultrasound image shows clearly delineated unenhanced area.
C, Late phase dynamic CT image shows slightly low-attenuation area in left lateral segment.

TABLE 3: Comparison of Numbers of Patients With Lesions Identified by Blinded Reviewers and Those Identified With Reference Standard (n = 191)

No. of Lesions Identified by Blinded Reviewers	Unenhanced Ultrasound	CEUS	DCT
Exceeded reference standard	13.1 (25)	31.9 (61)	18.8 (36)
Equal to reference standard	57.6 (110)	52.9 (101)	64.4 (123)
Fewer than reference standard	29.3 (56)	15.2 (29)	16.8 (32)

Note—Data are percentages. Numbers in parentheses are numbers of patients. Unenhanced ultrasound ultrasound and dynamic CT (DCT) but not contrast-enhanced (CEUS) are included in reference standard. Wilcoxon's signed rank test CEUS vs unenhanced ultrasound, $p < 0.001$; CEUS vs DCT, $p = 0.008$.

TABLE 4: Number of Lesions Detected Classified by Lesion Type

Classification	Reference Standard	Blinded Reviewers		
		Unenhanced Ultrasound	CEUS	DCT
Hepatocellular carcinoma	245	199	261	257
Metastasis	74	63	147	86
Hemangioma	38	32	37	31
Other benign lesion	11	11	12	10
Other malignant lesion	7	5	7	6
Total	375	310	464	390

Note—For metastasis, contrast-enhanced ultrasound (CEUS) vs unenhanced ultrasound, $p < 0.001$; contrast-enhanced ultrasound vs dynamic CT (DCT), $p < 0.001$ (Wilcoxon's signed rank test).

detected with CEUS was significantly larger than the number detected with DCT ($p < 0.001$). No significant difference was found between CEUS and DCT in the detection of lesions larger than 1 cm (Fig. 7).

Follow-Up of Newly Detected Lesions and Influence on Treatment Strategy

Among patients with newly visible lesions detected only with CEUS, 16 patients were available for follow-up, and the lesions in 12 patients were confirmed to be true lesions. Confirmation was verified at surgery in four cases, follow-up CT in four cases, follow-up MRI in two cases, follow-up angiography in one case, and needle biopsy in one case. All lesions in the other four patients were benign. Therefore, 75% (12 of 16) of cases were correctly diagnosed with CEUS. Table 5 shows the cases in which treatment strategy was changed on the basis of the diagnosis reached by the onsite investigators using CEUS. On the basis of information obtained on vascular or Kupffer images, the treatment strategy changed for 13 patients (6.8%).

Safety

No deaths, serious or severe adverse events were found in this study. The incidence of adverse events was 49.2% (95% confidence limits, 42.2%, 56.3%) (95 of 193 cases). Events with an incidence greater than 2% are shown in Table 6. The incidence of adverse drug reactions was 10.4% (95% confidence limits, 6.1%, 14.7%) (20 of 193 cases (Table 7). All adverse drug reactions were mild.

Discussion

The efficacy of CEUS with perflubutane microbubbles in the characterization and detection of lesions was assessed and compared with that of unenhanced ultrasound and DCT. Characterization of focal liver lesions relies on well-known vascular enhancement patterns at DCT and dynamic MRI, which are the standard methods of diagnosis [20]. Contrast enhancement with perfluorochemical microbubble agents in nonlinear ultrasound imaging, such as phase-modulation harmonic mode, has been found to be efficacious in various studies [21]. Because of the high temporal and spatial resolution of sonography, CEUS can depict the arterial perfusion characteristics of liver lesions and depict fine tumor vasculature. DCT has poorer performance than CEUS.

Differences in contrast enhancement patterns among lesion types have been well studied with several perfluorochemical microbubble agents, and CEUS has had high accuracy in characterization of lesions [22, 23]. Because contrast effects similar to those of other perfluorochemical agents are observed at CEUS with perflubutane microbubbles, it is not surprising that the accuracy of CEUS is higher than that of DCT. For example, although the number of cases was limited, the accuracy of CEUS in the diagnosis of hemangioma was 100%. Real-time CEUS depicted the typical enhancement pattern of hemangioma—namely, peripheral globular pooling of contrast material (cotton-wool appearance) followed by gradual perfusion of the entire

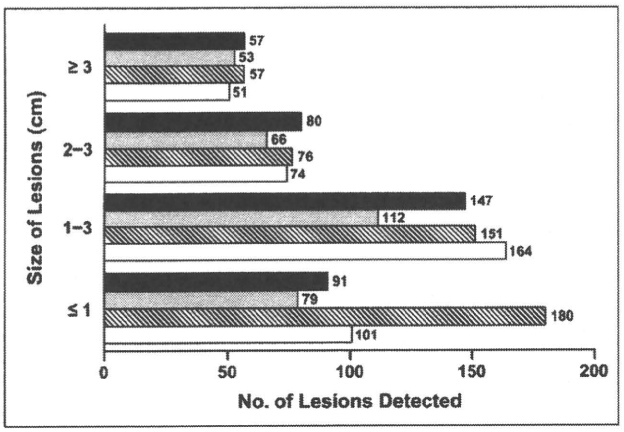

Fig. 6—Graph shows number of lesions classified according to lesion size detected by blinded reviewers using unenhanced ultrasound (*gray*), contrast-enhanced ultrasound (CEUS) (*striped*), and dynamic CT (*white*) and by onsite investigators using reference standard (*black*). Wilcoxon's signed rank test for lesions 1 cm or smaller, CEUS vs dynamic CT, $p = 0.008$; CEUS vs unenhanced ultrasound, $p < 0.001$; CEUS vs reference standard, $p = 0.001$.

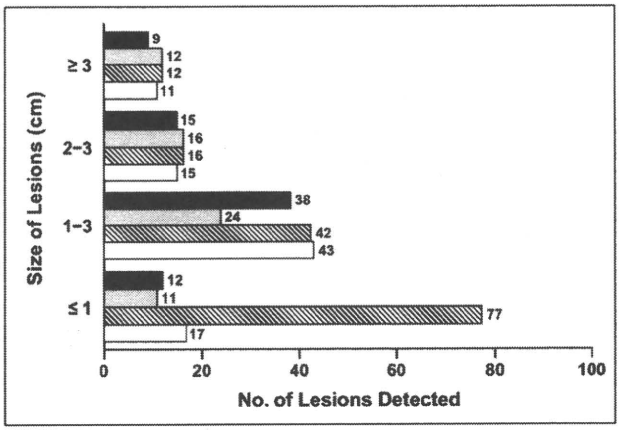

Fig. 7—Graph shows number of metastatic lesions classified according to lesion size detected by blinded reviewers using unenhanced ultrasound (*gray*), contrast-enhanced ultrasound (CEUS) (*striped*), and dynamic CT (*white*) and by onsite investigators using reference standard (*black*). Wilcoxon's signed rank test for lesions 1 cm or smaller, CEUS vs dynamic CT, $p < 0.001$; CEUS vs unenhanced ultrasound, $p < 0.001$; CEUS vs reference standard, $p < 0.001$.

TABLE 5: Changes in Treatment Strategy After Contrast-Enhanced Ultrasound Diagnosis

Treatment Planned Before Contrast-Enhanced Ultrasound	Treatment Planned After Contrast-Enhanced Ultrasound	No. of Patients
Radiofrequency ablation	Surgery	3
Radiofrequency ablation (RFA)	RFA (additional ablation)	2
Observation (benign lesion)	Surgery (malignant lesion)	2
Surgery (malignant lesion)	Observation (benign lesion)	1
Transcatheter arterial chemoembolization	Chemotherapy	1
Radiotherapy	Chemotherapy	1
Percutaneous ethanol injection therapy	Additional percutaneous ethanol injection therapy	1
Observation	Further examination	1
Bile duct stent	Transcatheter arterial chemoembolization	1

TABLE 6: Adverse Events (n = 193)

Event	No. of Patients
Fever	16 (8.3)
Nausea	13 (6.7)
Diarrhea	12 (6.2)
Malaise	11 (5.7)
Lumbar pain	10 (5.2)
Headache	9 (4.7)
Increased blood pressure	9 (4.7)
Abdominal pain	9 (4.7)
Thirst	7 (3.6)
Pain	7 (3.6)
Vomiting	7 (3.6)
Flank pain	6 (3.1)
Feeling of warmth	5 (2.6)
Enlarged feeling of abdomen	5 (2.6)
Omalgia	4 (2.1)
Dizziness	4 (2.1)
Decreased blood pressure	4 (2.1)
Epigastric pain	4 (2.1)
Injection site pain	4 (2.1)
Any adverse event	95 (49.2)

Note—Events with an incidence greater than 2% are listed. Some patients had more than one event. Values in parentheses are percentages.

lesion. Compared with unenhanced ultrasound, CEUS not only had approximately 20% greater overall accuracy but also was associated a higher degree of diagnostic confidence. Therefore, CEUS with perflubutane microbubbles is likely to be useful as a standard method of diagnosis and one that is comparable with DCT.

In terms of lesion detection, CEUS depicted more lesions than did DCT, many of which were small metastatic lesions (≤ 1 cm). Because of the high specificity of uptake of perflubutane microbubbles by Kupffer cells in normal parenchyma [16–18], malignant lesions that lack Kupffer cells are negatively enhanced. This characteristic, coupled with the higher spatial resolution of ultrasound, may explain the increased efficacy of CEUS in the detection of small lesions. SH U 508A (Levovist, Bayer Schering Pharma), an air-based microbubble agent, has been reported to have a parenchyma-specific contrast effect similar to that of perflubutane microbubbles, and this effect has been useful in detecting lesions [24, 25]. The parenchyma-specific contrast effect of SH U 508A is observed several minutes after injection, but it is effective only when imaging is performed at high acoustic power, and the effect is transient. Because imaging with SH U 508A entails destruction of microbubbles, visualization of the whole liver is limited to a single scan [26]. In contrast, because imaging with perflubutane microbubbles is performed at lower acoustic power without destruction of microbubbles, repeated scanning of the whole liver can be accomplished, as in our study. This capability may help operators reduce the number of missed lesions. Another technique that entails the use of Kupffer phase

TABLE 7: Adverse Drug Reactions (*n* = 193)

Event	No. of Patients
Albuminuria	3 (1.6)
Diarrhea	3 (1.6)
Neutropenia	2 (1.0)
Itching	1 (0.5)
Rash	1 (0.5)
Eruption	1 (0.5)
Headache	1 (0.5)
Stupor	1 (0.5)
Hypertension	1 (0.5)
Redness	1 (0.5)
Vomiting	1 (0.5)
Thirst	1 (0.5)
Increased lactate dehydrogenase level	1 (0.5)
Glycosuria	1 (0.5)
Peripheral ischemia	1 (0.5)
Thrombocytopenia	1 (0.5)
Hot flashes	1 (0.5)
Injection site pain	1 (0.5)
Any adverse reaction	20 (10.4)

Note—Values in parentheses are percentages. Some patients had more than one reaction.

imaging is contrast MRI with superparamagnetic iron oxide, which is also taken up by Kupffer cells [27, 28]. Although further studies are needed to compare CEUS with perflubutane microbubbles and MRI with superparamagnetic iron oxide, CEUS has the advantage of higher temporal and spatial resolution.

Most malignant tumors of the liver are HCC and metastatic lesions. HCC is one of a few malignant tumors in which the etiologic and pathogenic processes are understood and groups at high risk are well known. Chronic viral hepatitis leads to cirrhosis, which is a predisposing factor for HCC [29, 30]. This course is predominant in Asia. For early detection and treatment, it is recommended that these high-risk groups undergo ultrasound and DCT every 3 and 6 months, respectively [31]. Other groups at high risk are patients with alcoholic liver disease and, increasingly, those with fatty infiltration (nonalcoholic steatohepatitis) [32], which predominate in other parts of the world. Thus the need for early diagnosis of HCC is increasing. The liver also is a frequent site of metastasis. Strategies for the management of primary tumors and the prognosis are influenced by the absence or presence of hepatic metastasis, and early detection of these lesions is important.

Although it is the standard method of diagnosis of both types of liver tumors, DCT has limitations. First, radiation-induced cancer from CT examinations is becoming a major issue [33], and fewer CT examinations are being recommended. CT should be used only when the benefits outweigh the risks. Second, the sensitivity of DCT with helical CT in the detection of small metastatic lesions of the liver (≤ 1 cm) is 30–50% [34]. DCT with MDCT at collimation less than 5 mm does not have greater sensitivity for lesions 1.5 cm or smaller [35]. In this study, CEUS with perflubutane microbubbles was superior to DCT in both characterization and detection of focal liver lesions, especially in the detection of small hepatic metastatic lesions. The treatment of 13 of 191 patients (6.8%) was changed on the basis of the CEUS diagnosis. This finding suggests that current diagnostic procedures have room for improvement and that CEUS with perflubutane microbubbles may be an alternative to DCT.

In this study, patients with unenhanced ultrasound images of adequate quality were enrolled, and all the lesions imaged with unenhanced ultrasound were enhanced at CEUS without artifacts such as shadowing. This finding suggests that perflubutane microbubbles cause fewer artifacts. This effect may be attributed to the fact that the higher mechanical index can be applied for perflubutane microbubbles than for other perfluorochemical microbubbles, such as aqueous suspension of phospholipid-stabilized microbubbles filled with sulfur hexafluoride (SonoVue, Bracco) and perflutren (Definity, Lantheus Medical Imaging) owing to higher resistance to pressure [14].

The incidences of adverse events and adverse drug reactions were self-limited over the period of observation and were 49.2% and 10.4%, respectively. The relatively high incidence of adverse events can be attributed to adverse events caused by the primary disease, cancer, itself and by treatments and examinations after administration of perflubutane microbubbles. All adverse drug reactions were mild in intensity, and none was peculiar to perflubutane microbubbles. Therefore, the findings suggest that perflubutane microbubbles is a safe contrast agent.

A limitation of this study was potential bias affecting the blinded readings of DCT images because DCT was part of the reference standard. Despite this possible bias in favor of DCT, CEUS was more accurate than DCT in lesion characterization. This finding suggests that CEUS has potential as a diagnostic alternative to DCT for lesion characterization. Other limitations regarding DCT were that MDCT was not used at all centers and the slice thickness varied from 2 to 10 mm among the centers and was not standardized, although all were within routine CT protocols.

Another limitation was that not all newly detected lesions were followed up. Compared with the reference standard, 89 new lesions were detected only with CEUS in 61 patients. The onsite investigators tried to conduct follow-up, and 12 of 16 cases were confirmed to be true lesions. This finding suggests that CEUS has high potential in the detection of new true lesions. An additional limitation was the extent of the overall safety assessment. Although no serious adverse reactions, such as anaphylactic reaction or shock, were observed with perflubutane microbubbles in the 193 patients in this study or in more than 2,000 patients in clinical trials in the United States and Europe (unpublished data), further careful safety assessments are needed.

We conclude that compared with unenhanced ultrasound and DCT, CEUS with perflubutane microbubbles had better diagnostic efficacy in the characterization and detection of focal liver lesions with no substantial adverse drug reactions. CEUS with perflubutane microbubbles has potential as a diagnostic alternative to DCT in the care of patients with known or suspected focal liver lesions.

Acknowledgments

We thank K. Koito, T. Iwasaki, K. Sasaki, Y. Mizuguchi, N. Izumi, N. Ueno, T. Kumada, H. Gotoh, F. Urano, Y. Horiguchi, Y. Matsuda, S. Tanaka, Y. Kinoshita, M. Sata, S. Matsutani, M. Kudo, T. Hirai, A. Kono, A. Tanimoto, and T. Ichikawa, for data collection and assessment.

The 15 enrolling centers were Sapporo Medical University Hospital, Sapporo; Tohoku University Hospital, Sendai; National Cancer Center, Tokyo; Showa University Hospital, Tokyo; Tokyo Medical University, Tokyo; Musashino Red Cross Hospital, Musashino; Yokohama City University Hospital, Yokohama; Nagoya University Hospital, Nagoya; Fujita Health University Hospital, Toyoake; Toyohashi Municipal Hospital, Toyohashi; Ogaki Municipal Hospital, Ogaki; Osaka Medical Center for Cancer and

Cardiovascular Diseases, Osaka; Otemae Hospital, Osaka; Shimane University Hospital, Izumo; and Kurume University Hospital, Kurume.

References

1. Goldberg BB, Liu JB, Forsberg F. Ultrasound contrast agents: a review. *Ultrasound Med Biol* 1994; 20:319–333
2. Cosgrove D. Echo enhancers and ultrasound imaging. *Eur J Radiol* 1997; 26:64–76
3. Chomas JE, Dayton P, Allen J, Morgan K, Ferrara KW. Mechanisms of contrast agent destruction. *IEEE Trans Ultrason Ferroelectr Freq Control* 2001; 48:232–248
4. Kim TK, Han JK, Kim AY, Choi BI. Limitations of characterization of hepatic hemangiomas using a sonographic contrast agent (Levovist) and power Doppler ultrasonography. *J Ultrasound Med* 1999; 18:737–743
5. Klibanov AL, Ferrara KW, Hughes MS, et al. Direct video–microscopic observation of the dynamic effects of medical ultrasound on ultrasound contrast microspheres. *Invest Radiol* 1998; 33: 863–870
6. Schutt EG, Klein DH, Mattrey RM, Riess JG. Injectable microbubbles as contrast agents for diagnostic ultrasound imaging: the key role of perfluorochemicals. *Angew Chem Int Ed Engl* 2003; 42: 3218–3235
7. Lindner JR. Microbubbles in medical imaging: current applications and future directions. *Nat Rev Drug Discov* 2004; 3:527–532
8. de Jong N, Frinking PJ, Bouakaz A, Ten Cate FJ. Detection procedures of ultrasound contrast agents. *Ultrasonics* 2000; 38:87–92
9. Metoki R, Moriyasu F, Kamiyama N, et al. Quantification of hepatic parenchymal blood flow by contrast ultrasonography with flash-replenishment imaging. *Ultrasound Med Biol* 2006; 32:1459–1466
10. Burns PN, Wilson SR, Simpson DH. Pulse inversion imaging of liver blood flow: improved method for characterizing focal masses with microbubble contrast. *Invest Radiol* 2000; 35:58–71
11. Brannigan M, Burns PN, Wilson SR. Blood flow patterns in focal liver lesions at microbubble-enhanced US. *RadioGraphics* 2004; 24:921–935
12. Leen E, Ceccotti P, Kalogeropoulou C, Angerson WJ, Moug SJ, Horgan PG. Prospective multicenter trial evaluating a novel method of characterizing focal liver lesions using contrast-enhanced sonography. *AJR* 2006; 186:1551–1559
13. Nicolau C, Vilana R, Catalá V, et al. Importance of evaluating all vascular phases on contrast-enhanced sonography in the differentiation of benign from malignant focal liver lesions. *AJR* 2006; 186:158–167
14. Sontum PC. Physicochemical characteristics of Sonazoid, a new contrast agent for ultrasound imaging. *Ultrasound Med Biol* 2008; 34:824–833
15. Watanabe R, Matsumura M, Chen CJ, Kaneda Y, Ishihara M, Fujimaki M. Gray-scale liver enhancement with Sonazoid (NC100100), a novel ultrasound contrast agent: detection of hepatic tumors in a rabbit model. *Biol Pharm Bull* 2003; 26:1272–1277
16. Yanagisawa K, Moriyasu F, Miyahara T, Miyata Y, Iijima H. Phagocytosis of ultrasound contrast agent microbubbles by Kupffer cells. *Ultrasound Med Biol* 2007; 33:318–325
17. Watanabe R, Matsumura M, Munemasa T, Fujimaki M, Suematsu M. Mechanism of hepatic parenchyma-specific contrast of microbubble-based contrast agent for ultrasonography: microscopic studies in rat liver. *Invest Radiol* 2007; 42:643–651
18. Kindberg GM, Tolleshaug H, Roos N, Skotland T. Hepatic clearance of Sonazoid perfluorobutane microbubbles by Kupffer cells does not reduce the ability of liver to phagocytose or degrade albumin microspheres. *Cell Tissue Res* 2003; 312:49–54
19. Forsberg F, Piccoli CW, Liu JB, et al. Hepatic tumor detection: MR imaging and conventional US versus pulse-inversion harmonic US of NC100100 during its reticuloendothelial system-specific phase. *Radiology* 2002; 222:824–829
20. Winterer JT, Kotter E, Ghanem N, Langer M. Detection and characterization of benign focal liver lesions with multislice CT. *Eur Radiol* 2006; 16:2427–2443
21. Rettenbacher T. Focal liver lesions: role of contrast-enhanced ultrasound. *Eur J Radiol* 2007; 64: 173–182
22. Konopke R, Bunk A, Kersting S. The role of contrast-enhanced ultrasound for focal liver lesion detection: an overview. *Ultrasound Med Biol* 2007; 33:1515–1526
23. Quaia E, Calliada F, Bertolotto M, et al. Characterization of focal liver lesions with contrast-specific US modes and a sulfur hexafluoride-filled microbubble contrast agent: diagnostic performance and confidence. *Radiology* 2004; 232:420–430
24. Albrecht T, Blomley MJ, Burns PN, et al. Improved detection of hepatic metastases with pulse-inversion US during the liver-specific phase of SHU 508A: multicenter study. *Radiology* 2003; 227:361–370
25. Harvey CJ, Blomley MJ, Eckersley RJ, Heckemann RA, Butler-Barnes J, Cosgrove DO. Pulse-inversion mode imaging of liver specific microbubbles: improved detection of subcentimetre metastases. *Lancet* 2000; 355:807–808
26. Blomley MJ, Albrecht T, Cosgrove DO, et al. Improved imaging of liver metastases with stimulated acoustic emission in the late phase of enhancement with the US contrast agent SH U 508A: early experience. *Radiology* 1999; 210:409–416
27. Reimer P, Balzer T. Ferucarbotran (Resovist): a new clinically approved RES-specific contrast agent for contrast-enhanced MRI of the liver—properties, clinical development, and applications. *Eur Radiol* 2003; 13:1266–1276
28. Tanimoto A, Kuribayashi S. Application of superparamagnetic iron oxide to imaging of hepatocellular carcinoma. *Eur J Radiol* 2006; 58:200–216
29. Parikh S, Hyman D. Hepatocellular cancer: a guide for the internist. *Am J Med* 2007; 120:194–202
30. Okita K. Clinical aspects of hepatocellular carcinoma in Japan. *Intern Med* 2006; 45:229–233
31. Kobayashi K, Terasaki S, Matsushita E, Kaneko S. Strategy of early diagnosis. *Kan-Tan-Sui Frontier* 1999; 5:57–59
32. Bruix J, Sherman M. Diagnosis of small HCC. *Gastroenterology* 2005; 129:1364
33. Berrington de González A, Darby S. Risk of cancer from diagnostic x-rays: estimates for the UK and 14 other countries. *Lancet* 2004; 363:345–351
34. Bluemke DA, Sahani D, Amendola M, et al. Efficacy and safety of MR imaging with liver-specific contrast agent: U.S. multicenter phase III study. *Radiology* 2005; 237:89–98
35. Haider MA, Amitai MM, Rappaport DC, et al. Multi-detector row helical CT in preoperative assessment of small (< or = 1.5 cm) liver metastases: is thinner collimation better? *Radiology* 2002; 225:137–142

ELSEVIER

Clinical Imaging 33 (2009) 447–453

CLINICAL IMAGING

Perfusion study of liver lesions with superparamagnetic iron oxide: distinguishing hepatocellular carcinoma from focal nodular hyperplasia

Kazuhiro Saito*, Katsutoshi Sugimoto, Ryota Nishio, Youichi Araki, Fuminori Moriyasu, Dai Kakizaki, Koichi Tokuuye

Department of Radiology, Tokyo Medical University, Tokyo, Japan
Department of Internal Medicine, Tokyo Medical University, Tokyo, Japan

Received 10 November 2008; accepted 14 January 2009

Abstract

We performed a perfusion study with superparamagnetic iron oxide (SPIO) and evaluated the possibility of acquiring hemodynamic imaging in hypervascular hepatocellular nodules. Single-slice computed tomography during arteriography (SCTA) and an SPIO perfusion study were performed and compared. The findings of the direction of blood flow in the lesion and the findings corresponding to the corona enhancement on the SPIO perfusion study agreed well with the findings of SCTA. In conclusion, SPIO perfusion is useful in evaluating the hemodynamics of hypervascular hepatocellular nodules.

Keywords: Corona enhancement; Dynamic study; MRI; SPIO

1. Introduction

Both hepatocellular carcinoma (HCC) and focal nodular hyperplasia (FNH) show hypervascular characteristics on diagnostic imaging. Typically overt HCC shows tumor enhancement in the arterial phase and washout in the equilibrium phase on dynamic computed tomography (CT) and magnetic resonance imaging (MRI) and has capsule-like structure around the tumor [1,2]. FNH is usually lobulated and well circumscribed and has a central stellate scar with radiating fibrous septa. Dynamic study shows enhancement in the arterial phase and isodensity in the equilibrium phase [3,4]. In cases with completely typical findings, the differential diagnosis of both entities is relative easy, but in cases that do not have completely typical findings, the diagnosis is difficult.

FNH displays a specific centrifugal enhancement on angiography, called a spoke-wheel appearance [5]. While this finding can be detected in 57–90% of patients with large lesions, it can be difficult to detect in small lesions [5,6]. Kudo et al. [7] reported excellent detection of this specific vascular structure with dynamic contrast-enhanced ultrasound under infusion of carbon dioxide microbubbles through an angiographic catheter. Miyayama et al. [8] reported the possibility of the detection of these specific hemodynamic features with continuous acquisition of single-slice CT during arteriography (SCTA). However, these methods have the drawback of acquiring invasive angiography. SCTA also shows the drainage vessel indirectly [8,9]. The drainage vessel of hypervascular HCC is the portal vein, and SCTA shows corona enhancement around a tumor [9]. However, the drainage vessel of FNH is the hepatic vein or sinusoid around the nodule [10], and corona enhancement is not always observed.

Superparamagnetic iron oxide (SPIO)-enhanced MRI is a noninvasive modality. SPIO accumulates in Kupffer cells present in normal liver parenchyma and causes a signal loss

* Corresponding author. Tokyo Medical University, 6-7-1 Nishi-Shinjuku, Shinjuku-ku, Tokyo 160-0023, Japan. Tel.: +3 3342 6111; fax: +3 3348 6314.

0899-7071/09/$ – see front matter © 2009 Elsevier Inc. All rights reserved.
doi:10.1016/j.clinimag.2009.01.008